



LAWRENCE
LIVERMORE
NATIONAL
LABORATORY

Identifying divertor detachment using a machine learning model trained on divertor camera images from DIII-D

B. S. Victor, F. Scotti

August 9, 2024

25th Topical Conference on High Temperature Plasma
Diagnostics
Asheville, NC, United States
April 21, 2024 through April 25, 2024

Disclaimer

This document was prepared as an account of work sponsored by an agency of the United States government. Neither the United States government nor Lawrence Livermore National Security, LLC, nor any of their employees makes any warranty, expressed or implied, or assumes any legal liability or responsibility for the accuracy, completeness, or usefulness of any information, apparatus, product, or process disclosed, or represents that its use would not infringe privately owned rights. Reference herein to any specific commercial product, process, or service by trade name, trademark, manufacturer, or otherwise does not necessarily constitute or imply its endorsement, recommendation, or favoring by the United States government or Lawrence Livermore National Security, LLC. The views and opinions of authors expressed herein do not necessarily state or reflect those of the United States government or Lawrence Livermore National Security, LLC, and shall not be used for advertising or product endorsement purposes.

Identifying divertor detachment using a machine learning model trained on divertor camera images from DIII-D

B. S. Victor¹ and F. Scotti¹

Lawrence Livermore National Laboratory, Livermore, CA 94550, USA

(*Electronic mail: victorb@fusion.gat.com)

(Dated: 15 July 2024)

This paper describes the application of a machine learning (ML) algorithm using a convolution neural network, first developed in Ref. 1, to detect divertor detachment in DIII-D. Detachment detection is based on images from tangentially viewing upper and lower filtered divertor cameras that measure CIII emission at 465 nm. Separate ML models are developed for lower single null (LSN) and upper single null (USN) configurations with mostly closed divertor shapes. Due to the viewing angle and divertor geometry, camera images of the upper divertor show a stark contrast in CIII emission between attached and detached conditions and the model identified detachment with 100% accuracy in the test data set. For the lower divertor images, the contrast between attached and detached conditions is lower and the model identifies detachment with 96% accuracy. This ML model will be applied to the image data after each shot to provide a rapid assessment of divertor detachment to aid operation of DIII-D with the potential extension to other devices in the future.

I. INTRODUCTION

Future high-power plasma devices will need to limit peak heat flux to stay within the material limits of the divertor. One approach being developed on existing tokamaks is divertor detachment—where the primary plasma boundary interaction is moved away from the divertor target surface². Detachment creates a low temperature buffer region between the plasma and the divertor plasma-facing components, limiting the heat flux to the material surface. As the temperature changes, the dominant emission in the divertor region changes. This change in emission can be measured with visible-wavelength cameras. Detachment can be inferred using tomographic inversion of divertor image data to generate 2D maps of local emissivity³. To automate the detachment identification process, a machine learning (ML) algorithm using a convolution neural network (CNN), first developed in Ref. 1, determines detachment based upon images of filtered impurity emission from tangentially viewing divertor cameras (Tangential TV⁴). In this paper, the ML model has been applied to raw images, before any optical corrections or processing, and extended to additional plasma configurations to develop a rapid method for detachment detection.

DIII-D is capable of positioning the strike points over a wide range of locations in the upper or lower divertor. The strike points are defined as the locations where the last closed flux surface connects to the divertor through the X-point. Plasmas biased downward with a single X-point in the lower divertor are considered lower single null (LSN) and biased upward with a single X-point in the upper divertor are upper single null (USN). Tangentially-viewing TV cameras with band-pass filters to isolate a small wavelength range are focused on both the upper and lower divertors⁵. Detachment experiments are performed in both LSN and USN in order to test scenario operation with heat flux control consistent with maintaining the integrity of the wall armor. Ref. 1 details the initial detachment identification using LSN plasmas with the outer leg strike point on the ‘Shelf’ as indicated in Fig. 1. This work

extends the analysis to LSN plasmas with the outer leg strike point on the ‘Floor’ and plasmas in an USN configuration as shown in Fig. 1.

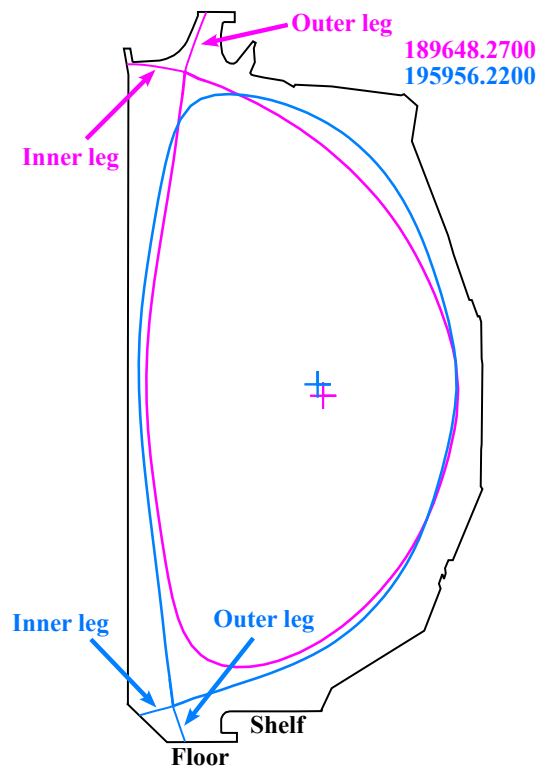


FIG. 1. Last closed flux surfaces for LSN (blue, shot 195956) and USN (magenta, shot 189648) equilibria. The inner and outer legs between the X-point and the intersection points on the divertor are labeled. The poloidal cross-section of the DIII-D wall is outlined in black.

In addition, these models are combined into a single workflow that will run automatically between discharges on DIII-D. This provides feedback on whether detachment has been achieved within minutes after each shot and helps to guide

operation of the machine without relying on tomographic inversion of the images.

This paper is organized as follows: Section II describes the plasma configuration, the tangential TV diagnostic, and includes example images used to train the ML model. Section III describes how the ML model is trained and gives a description of the CNN used in the ML model. The performance of the ML model when applied to test discharges is evaluated in Section IV. Finally, Section V discusses application of the model for between shot analysis of detachment and concludes the paper.

II. EXPERIMENT AND DIAGNOSTIC DESCRIPTION

The tangential TV diagnostics on DIII-D measures spectral emission in the divertor regions of the plasma, with sensitivity throughout the visible spectral range. In this work, a bandpass filter isolates emission from C III at 465 nm, where carbon is the primary radiator in the plasma due to the graphite divertor and walls on DIII-D. CIII emission is one of the brightest features in the visible wavelength range, allowing for good signal level at high acquisition speed. Peak emissivity of CIII occurs between 8 and 12 eV. When the divertor plasma is “attached” the target plasma temperature is ~ 10 eV and a dominant region of CIII emission is apparent where the plasma strikes the divertor. As the plasma detaches, the temperature of the plasma at the divertor target drops to ~ 2 eV. This ‘detachment cliff’⁶ leads to a rapid drop in CIII emission at the strike point and the brightest emission in the images moves away from the divertor and diffuses. Thus, there are two distinct states with the brightest emission either on or away from the divertor surface, that are used to train the neural network. Note that all of these discharges are with the ion $\vec{B} \times \nabla B$ direction into the divertor, which leads to a sharper transition in the strike point temperature during detachment⁶.

In the current work, divertor detachment has been analyzed in the two plasma shapes shown in Fig. 1: high triangularity USN (magenta trace, shot 189648) with the strike point on the ceiling and high triangularity LSN (blue trace, shot 195956) with the strike point on the floor. The dominant CIII emission in attached plasmas occurs where the inner and outer legs strike the divertor. The outer leg is the strike point location at larger major radius. The raised surface of the lower divertor, with $Z = -1.25$ m, is referred to as the shelf and the inner portion the floor, $Z = -1.36$ m. The strike point is considered to be on the floor when the strike point of the outer leg is on the floor and the inner leg is near or on the inner wall.

Fig. 2 shows a sample view into the DIII-D device from the tangential TV cameras, with a plasma in both attached (a) and detached (b) conditions for an USN discharge. A CAD-based model of the graphite tiles that make up the first wall of DIII-D is overlaid in the view to indicate the 3D nature of the view from the cameras. These are line-integrated images so they do not directly map to the poloidal cross section shown in Fig. 1. Abel inversions, which map the camera images to the 2D cross sections, can be used to infer detachment³; however, this process can be resource intensive so cannot be done quickly after

each shot. A rough indication of the inner and outer strike points have been indicated in Fig. 2 to aid in interpreting the images. The locations of the strike points have not changed between Fig. 2(a) and (b), but the location of the dominant emission has moved away from the strike points. When the plasma is attached, Fig. 2(a), the brightest emission, indicated by the dark red level of the colormap, is at the outer leg strike point. Emission is also apparent near the inner leg strike point, indicated by green through orange levels of the colormap. After the plasma detaches, the dominant emission, indicated in red, is located in the lower right portion of the red rectangle in Fig. 2(b). Thus the location of the dominant emission has changed from near the outer leg strike point to a region away from either strike point.

Fig. 3 shows attached (a) and detached (b) conditions for a LSN plasma with the strike point on the floor. The distinction between attached and detached conditions is not as straightforward to identify for LSN plasmas with the strike point on the floor. When attached, Fig. 3(a), emission along the outer strike point, indicated in green through red levels of the colormap, follows the divertor toroidally. After detachment, Fig. 3(b), the emission becomes less diffuse and appears to move inward from the outer strike point toward smaller radius. Along the inner strike point, the distance between the toroidal emission, indicated in green, and the toroidal circle that connects the angled divertor tiles to the inner wall increases between attached, Fig. 3(a), and detached, Fig. 3(b), conditions. Despite the difference in the light emission between the two images, the location of the inner and outer strike points, as indicated by the magnetic equilibrium, remain the same. Ultimately, one value of the ML algorithm is its ability to distinguish differences between images that are difficult to differentiate by eye.

III. TRAINING THE ML MODEL

The ML model for divertor detachment based on the tangential TV data was originally developed by Boyer, *et al.* in Ref. 1. This work builds off that model and demonstrates its inherent flexibility by successfully expanding to different cameras and strike point locations. In addition, this work is focused on developing a workflow for between shot analysis. For this reason, the ML models are trained on raw images before any transformations, such as corrections for alignment and spherical aberration³, have been applied. In each strike point configuration, a subsection of the image is selected and / or the image is downsampled to reduce the computation resources necessary to evaluate and apply the model.

Separate ML models are developed for each configuration. Images from each strike point configuration are divided into three groups of roughly: 70% training, 15% validation, and 15% testing. The images are labeled based on either direct inspection of the images based on past experience or tomographic inversion³ of the raw images. The training set is used to generate the initial ML model. The model is then tested on the validation data. This is done through a series of ~ 50 iterations. If the error in the fit to the validation set of images

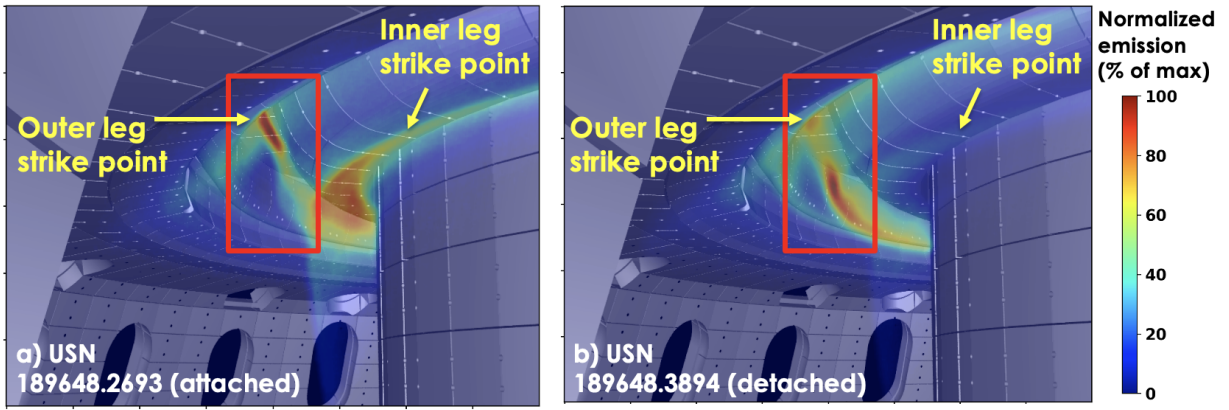


FIG. 2. The peak emission moves away from the strike point locations when the plasma detaches. Both images are from the tangential TV camera viewing the upper divertor. (a) shows the brightest emission near the strike points. (b) shows the brightest emission has moved away from the strike points. The red rectangles indicate the region of the image used to train the ML model.

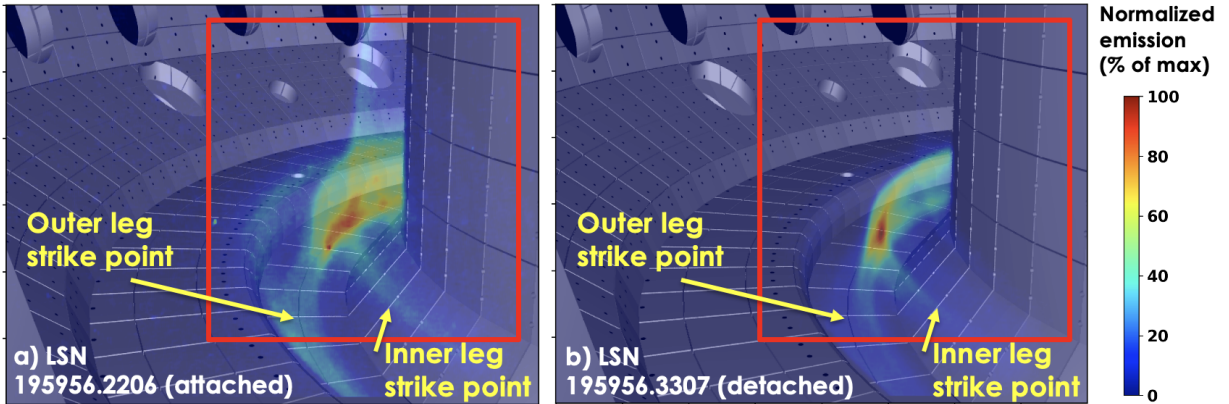


FIG. 3. Emission near the divertor tiles decreases when the plasma detaches. Both images are from the tangential TV camera viewing the lower divertor. (a) emission is seen along the strike point locations. (b) peak emission has moved away from the strike points. The red rectangles indicate the region of the image used to train the ML model.

decreases by any amount with a subsequent iteration then the new model replaces the previous model. This helps to prevent overfitting and ensure that the model is generalizable to a larger number of images.

A. Description of the convolution neural network

This section gives an overview of the CNN architecture used to create the ML model. The ML model was developed using PyTorch⁷ within Python.

A convolution layer is used here to detect patterns in images. In the first convolution layer below, 16 filters are applied to the input grayscale images using a 3x3 kernel with a pixel stride of one. During training, these filters evolve to extract the most important data from the image. The outputs of the convolution layer are called feature maps. 16 feature maps are created in the first convolution layer. A second convolution layer is used to extract more complex features from the image. Each pass of a convolution layer with kernel size 3

reduces the width and height of the image by one.

After each convolution layer, a Rectified Linear Unit (ReLU) is applied to the feature maps. Each value in the feature map arrays are considered ‘nodes’. The ReLU introduces non-linearity to the model by setting all nodes with negative values in the feature map to zero. All positive nodes remain unchanged. Thus, the ReLU is used to determine which nodes in the NN model remain active.

The max-pooling layer decreases the spatial dimension of the outputs from previous steps. In this case, the max-pooling layer selects the maximum value in each 2x2 region, thereby reducing the width and height of the feature maps by 50%. Max-pooling layers reduce the complexity of the model while maintaining the most important features.

Dropout layers are used to prevent overfitting. For the first dropout layer, 25% of the nodes output from the max-pooling layer are set to 0. This helps the model find more robust features that generalize beyond the training set.

Next, the two-dimensional feature maps are flattened into a one-dimensional vector to transition from multiple convo-

lution layers to a single-layer feed-forward network. While relatively simple, single-layer feed-forward networks are useful for binary classification problems such as determining divertor detachment. Single-layer means there is a direct connection from input to output, no hidden layers. Feed-forward means the data propagates in only one direction through the network. A ReLU layer is used again to introduce nonlinearity by setting all negative values in the output to zero. The second single-layer feed-forward network reduces the dimensionality to two, which maps the features of the model to the two possible outputs.

Finally, the softmax function converts the output of the network to a probability that the original image represents an attached or detached divertor. In this work, the output with highest probability is taken as the model's prediction.

IV. MODEL RESULTS

After training and validation, the models are applied to test data to determine the accuracy of the model. Accuracy is determined by the F1 score⁸, defined as

$$F_1 = \frac{t_p}{t_p + \frac{1}{2}(f_p + f_n)} \quad (1)$$

where t_p are true positives (the model predicts detachment and the experiment is detached), f_p are false positives (the model predicts detachment and the experiment is attached), and f_n are false negatives (the model predicts attached conditions and the experiment is detached). The ratio $t_p/(t_p + f_p)$ is known as the precision, and is a measure of accuracy of the predicted detached states from the model. The ratio $t_p/(t_p + f_n)$ is known as the recall, and is a measure of how many of the actual detached states are predicted by the model. Taken together, the 'F1 score is the harmonic mean of precision and recall'⁸.

For the USN strike point images, there is a distinct difference between attached and detached times that is apparent in the raw images. Thus, even with a limited data set, the model can accurately differentiate between attached and detached conditions. Using 800 time slices across five shots to train and validate a detachment detection ML model for the upper divertor, an F1 score of 100% was achieved on two test shots, Fig. 4. An F1 score of 100% indicates that all time points in a shot were accurately predicted by the model. In both discharges, the plasma detaches for a period before becoming re-attached later in the discharge. Both transitions were accurately captured by the model. Fig. 4 shows a difference in the detachment conditions at different plasma current. At lower plasma current, the plasma detaches at lower density and remains detached until the density decreases later in the discharge. At higher plasma current, detachment occurs at higher density and the plasma re-attaches despite remaining at higher density.

The contrast between attached and detached divertors is not as distinct in the LSN floor discharges. Labeling the discharges was also more challenging and required performing tomographic inversions to calculate the location of the detachment front. The plasma is considered detached when the de-

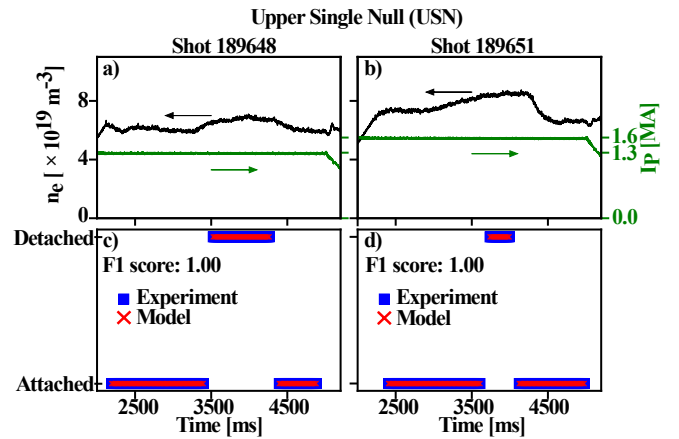


FIG. 4. High accuracy is achieved in the USN ML model when evaluating testing data, panels (c) and (d). Detachment occurs in shot 189648, panels (a) and (c), when the density increases. For the higher plasma current discharge (shot 189651), detachment occurs at a higher plasma density than the lower plasma current shot, panels (b) and (d).

tachment front is more than ≈ 2 cm away from the surface of the divertor. Labeling individual time slices, as opposed to specifying time ranges in the USN discharges mentioned previously, allows a change in the workflow such that the training, testing, and validation sets were split up by time slice instead of shot. A total of 1460 images across 12 shots, containing 1074 attached times and 386 detached times, were used for training, testing, and validation. Predictions from the ML model on LSN shots are presented in Fig. 5, which shows a decrease in accuracy, as indicated by the F1 score, relative to the USN shots. The detachment front location, as calculated by tomographic inversion³, is also included in the figure. The accuracy of the machine learning algorithm is lowest when the detachment front is closest to the floor at $Z = -1.36$ m, between 2600-2700 ms in Shot 195956, or when the plasma has just reattached, between 3800-4000 ms in Shot 195952. The location of the X-point, which is approximately stationary through the analysis period, is also included. Comparing the detachment front location to the X-point shows that the detachment front for Shot 195956 is at the X-point, while for shot 195952, the detachment front never fully reaches the X-point. When looking across all analyzed shots with the strike point on the floor, the cumulative F1 score is 96%. The sparser test data set in Fig. 5 compared to Fig. 4 is due to each shot being split into test, training, and validation data sets. The displayed points are from the test data set.

V. DISCUSSION AND FUTURE WORK

Edge localized modes (ELMs) complicate the interpretation of these divertor images. During an ELM, the plasma can burn through the detached region causing the plasma to temporarily reattach. The tangential TV cameras operate at 60 Hz so the images integrate through an ELM period. Thus time

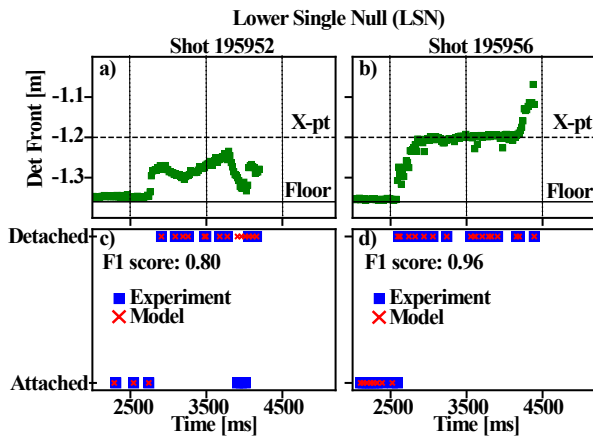


FIG. 5. Accuracy of 80% and 96% is achieved in two LSN shots from the testing data set, panels (c) and (d). The detachment front locations, panels (a) and (b), is determined by tomographic inversion of the images. Accuracy is lower when the detachment front is close to the divertor target on the floor at -1.36 m.

ranges during a discharge that are predominantly detached will still have CIII emission from the divertor surface during these short periods of reattachment. This does not typically create a problem interpreting the images as there still is an apparent difference between times with and without detachment.

A primary goal in developing these ML models is to implement an analysis script to run automatically between shots. This workflow has been developed and will be implemented during the upcoming DIII-D campaign. After each discharge, images from upper and lower tangential TV cameras will be evaluated using the ML model developed for the respective divertor configuration. This will produce binary outputs indicating 0-attached or 1-detached as a function of time for the two lower divertor models and the one upper divertor model. Next, the equilibrium will be analyzed to select the divertor configuration based on the up/down position of the plasma and the location of the outer leg strike point. The divertor configuration, which can change in time, will then be used to determine the final output of attached and detached conditions.

Consideration was given to using transfer learning⁸ to adapt one ML model to another. However, due to the relative speed a new model can be developed, training new models from scratch proved to be more straightforward.

New detachment models will be developed as changes are made to the DIII-D divertors. During the previous maintenance period, the upper divertor in DIII-D was moved closer to the inner wall (lower major radius) to allow operation at increased triangularity. As new data becomes available in this divertor configuration, a new ML model for detachment detection will be developed. The relative ease in developing new ML models based on divertor images bodes well for their application to other tokamaks and future devices. One question that will need to be addressed is the optimal impurity emission to view in devices without a carbon wall/divertor.

In conclusion, this paper has presented an extension of the

ML model developed in Ref. 1. First, the model has been trained directly on the raw images to allow for rapid application of the model on a between-shot basis. This will enable session leaders to make informed decisions to control detachment during experiments. ML models have also been developed for plasmas in USN and LSN floor configurations. This represents a majority of the operational scenarios on DIII-D. These new models will be implemented for between-shot analysis of divertor detachment during the upcoming run period on DIII-D.

VI. ACKNOWLEDGMENTS

Use of data from DIII-D experiments performed by A. Moser and H. Wang is gratefully acknowledged. The authors are also thankful for the contributions from the DIII-D team.

This work was performed under the auspices of the U.S. Department of Energy by Lawrence Livermore National Laboratory under Contract DE-AC52-07NA27344. This material is based upon work supported by the U.S. Department of Energy, Office of Science, Office of Fusion Energy Sciences, using the DIII-D National Fusion Facility, a DOE Office of Science user facility, under Award DE-FC02-04ER54698.

Disclaimer: This report was prepared as an account of work sponsored by an agency of the United States Government. Neither the United States Government nor any agency thereof, nor any of their employees, makes any warranty, express or implied, or assumes any legal liability or responsibility for the accuracy, completeness, or usefulness of any information, apparatus, product, or process disclosed, or represents that its use would not infringe privately owned rights. Reference herein to any specific commercial product, process, or service by trade name, trademark, manufacturer, or otherwise does not necessarily constitute or imply its endorsement, recommendation, or favoring by the United States Government or any agency thereof. The views and opinions of authors expressed herein do not necessarily state or reflect those of the United States Government or any agency thereof.

VII. DATA AVAILABILITY STATEMENT

The data that support the findings of this study are available from the corresponding author upon reasonable request.

- ¹M. D. Boyer *et al.*, “Classification and prediction of detachment in DIII-D using neural networks trained on C III imaging,” Submitted to Nuclear Fusion (2024).
- ²A. W. Leonard, “Plasma detachment in divertor tokamaks,” *Plasma Physics and Controlled Fusion* **60**, 044001 (2018).
- ³W. H. Meyer *et al.*, “Tomographic analysis of tangential viewing cameras (invited),” *Review of Scientific Instruments* **89**, 10K110 (2018).
- ⁴M. E. Fenstermacher *et al.*, “A tangentially viewing visible TV system for the DIII-D divertor,” *Review of Scientific Instruments* **68**, 974–977 (1997).
- ⁵D. G. Nilson *et al.*, “A tangentially viewing vacuum ultraviolet TV system for the DIII-D divertor,” *Review of Scientific Instruments* **70**, 738–741 (1999).
- ⁶A. McLean *et al.*, “Electron pressure balance in the sol through the transition to detachment,” *Journal of Nuclear Materials* **463**, 533–536 (2015).
- ⁷A. Paszke *et al.*, “Pytorch: An imperative style, high-performance deep learning library,” in *Advances in Neural Information Processing Systems*, Vol. 32 (Curran Associates, Inc., 2019).
- ⁸A. Geron, *Hands-On Machine Learning with Scikit-Learn, Keras, and TensorFlow: Concepts, Tools, and Techniques to Build Intelligent Systems*, 2nd ed. (O’Reilly Media, Inc., 2019).